Zero Kinetic Energy Photofragment Spectroscopy: The Threshold Dissociation of NO_2

J. A. Mueller, S. A. Rogers, and Paul L. Houston*

Department of Chemistry, Cornell University, Ithaca, New York 14853-1301

Received: June 5, 1998; In Final Form: September 14, 1998

A new type of photofragment spectroscopy has been developed and applied to the photodissociation of NO_2. Photofragments with zero recoil kinetic energy are selectively detected as the total energy of the dissociating system is varied. The resulting spectra provide information about the transitions that occur between energy levels of the transition state and energy levels of the final products. With proper calibration of the laser wavelength, the method may be useful in the accurate identification of the dissociation threshold. The technique is demonstrated by the detection of O atoms from the near-threshold photodissociation of NO_2. A sharp onset of signal occurs at the dissociation threshold of, while for higher energies, a new peak occurs as the energy threshold is reached for each possible NO internal state. An analysis of the intensity distribution of the spectral peaks suggests that the maximum orbital angular momentum allowed by the 0.5 cm^{-1} resolution of the instrument is near $5\hbar$, implying that the centrifugal barrier for that value of the angular momentum is less than or equal to 0.5 cm^{-1}.

I. Introduction

A new spectroscopic technique has been developed which involves probing only the very low kinetic energy fragments of a dissociation as a function of photolysis energy. Called zero kinetic energy (ZKE) photofragment spectroscopy, the technique is most useful in dissociations for which there is no barrier to the recombination of the products, as is often the case in systems that decompose to give radicals. ZKE photofragment spectroscopy allows observation of fragments just as they become energetically accessible, so several useful applications of the technique are possible. First, thresholds for dissociation can be determined to within a fraction of a wavenumber. Second, conservation of energy and momentum can be used to determine the rotational and vibrational level structure of one fragment from the ZKE spectrum of the sibling fragment. Consequently, the technique could prove useful in assigning the spectra of unstable radicals. Finally, as shown in this work, the magnitude of the ZKE signal can be monitored as a function of wavelength to look for deviations from statistical distributions. Such deviations provide information about the size of centrifugal barriers along the reaction coordinate.

NO_2 was chosen as a test case for the new technique because it is known not to have a barrier to the NO+O recombination and because there have been many previous studies examining its dissociation behavior near threshold. Despite its small size, the electronic state structure and dissociation dynamics of the nitrogen dioxide molecule are complex. Since so much effort has been expended in elucidating various aspects of the behavior of NO_2, it is not possible to give a complete review; only a summary of the most relevant work will be given here.

Careful measurement[1] of the dissociation energy of NO_2 from its ground rotational and vibrational level has yielded $D_0 = 25128.57 \pm 0.05$ cm^{-1}. This value is in excellent agreement with that measured by Butenhoff and Rohlfing,[2] and differs slightly from the value obtained by Robra et al. a few years earlier.[3]

At energies high above the dissociation threshold, the lifetime of the excited NO_2 molecule is shorter than the rotational period, so information about the excited state can be obtained by measuring the product angular distribution and the alignment of the rotational angular momentum with respect to the fragment recoil velocity.[4−9] Values of the anisotropy parameter β in the range from 0.6 to 1.8 were obtained for dissociation wavelengths between 347 and 360 nm. The differences between the anisotropy parameters can be largely reconciled by taking into account the differences in rotational temperature at which the various experiments were performed.[6] Nearer to the dissociation threshold, Butenhoff and Rohlfing[2] have used transient grating spectroscopy to measure the anisotropy of the recoil for states at an excess energy of 125.9 cm^{-1}. They find values ranging from $\beta = 0.36$ to $\beta = 1.5$. The effective value of β decreased with decreasing translational energy available to the products. These studies indicate that the absorption in this wavelength region occurs from the X^2A_1 state to the 1^2B_2 electronic state, with less than 5% contribution from absorption to the $^2B_1$ state, which is also energetically accessible.[4]

Theoretical calculations by Gillispie et al.[12] and by Jackels and Davidson[13,14] showed that the $^2A_1$ and $^2B_2$ states are strongly coupled through the asymmetric stretch, so that a conical intersection exists between the states. As a result of this very strong vibronic coupling, the molecular eigenstates excited are an admixture of the zeroth-order $^2B_2$ and X^2A_1 vibronic levels. Further theoretical investigations[15,16] of the region of the conical intersection and the effect it has on the spectroscopy of nitrogen dioxide have been carried out; they complement the extensive experimental spectroscopic studies carried out primarily by Delon, Jost and co-workers[17−20] and Miyawaki et al.[21]

Delon, Jost, and co-workers[17−20] and Ionov et al.[22] have noted that the density of states of NO_2 increases dramatically a few wavenumbers below the threshold for NO + O production. A possible interpretation of this observation is that even potentials correlating to $O(^3P_2) + NO(^2\Pi)$, which are repulsive at short range, may have shallow van der Waals minima at long range. This fact will be important in relating the size of the centrifugal barriers obtained in this work to the calculated long-range potential for NO + O.

10.1021/jp982634m CCC: $15.00
Published on Web 10/27/1998

Steplike increases of the rate constant for the NO_2 dissociation as a function of energy in excess of the threshold have been observed by Wittig and co-workers.[23,24] The time-domain experiment, which measured the rate constant 0− ∼800 cm^{-1} above the dissociation threshold, employed sub-picosecond lasers with bandwidth of 20 and 80 cm^{-1}. Steps in a plot of the rate constant as a function of excitation energy were observed in the region between 0−300 cm^{-1} above the dissociation threshold. The steps, spaced by ∼100 cm^{-1}, are believed to arise from the opening of accessible transition state energy levels. A curious feature of the results is the comparatively large spacing of the increases. Reactions for which there is no barrier to recombination of the radical products typically display the characteristics of a "loose" transition state.[25] That is, the transition state is located far out on the reaction coordinate where the separation between the two fragments is comparatively large and the bending vibrational motion of the parent molecule has evolved almost completely to the rotational and translational motion of the fragment species. In such a case, the energies of the transition state levels are very close to those describing the free rotational motion of the fragments. The fundamental frequency of the NO_2 bending mode is 758.64 cm^{-1} [26] and the 1.696115 cm^{-1} rotational constant of NO in the ground electronic state[27] means that the first few rotational levels are separated by only a few wavenumbers. In comparison, the ∼100 cm^{-1} spacing of the transition state levels is quite large, implying much "tighter" character in the transition state than one might at first expect.

Experimental studies of the NO_2 dissociation rate close to the threshold (0−150 cm^{-1}) were carried out by Miyawaki et al.[28] by monitoring the PHOFEX spectrum of the O or NO product. By measuring the linewidths of peaks in the PHOFEX spectrum, they observed steplike increases in the rate constant with spacing corresponding to the first few rotational levels of the NO product, an observation that implies that the transition state is indeed loose, as originally expected.

The Miyawaki results initially seemed to be at odds with the findings of the Wittig group, but the conflict[29,30] has apparently been resolved by the variational RRKM calculations of Klippenstein and Radivoyevitch.[31] Their study combined an ab initio calculation of the O−NO interaction potential in the region of the transition state in order to determine, as a function of excitation energy, the interfragment separation at which the transition state is located. The calculations show that although the transition state is indeed loose at energies very close to the dissociation threshold (<∼10 cm^{-1}), it tightens up very rapidly as the energy of the excited molecules increases, moving to a fragment separation distance of about 3.0 Å when the excitation energy is 100 cm^{-1} above the dissociation threshold. The spacing of the evolving bending/hindered rotation mode at that excitation energy is about 50−80 cm^{-1}, in reasonable agreement with the results obtained in the Wittig group.

Ab initio calculations accounting for the effect of spin−orbit interactions on the intermolecular potential have been performed by Katagiri and Kato.[32] They also calculated the spacing between the bending/rotation levels along the reaction coordinate. It was found that only the lowest two of these states are purely attractive; the rest all have a barrier to the O−NO recombination reaction. At O−NO separations of about 3.0 Å, the spacing between the evolving vibrational levels was found to be about 60−80 cm^{-1}, in excellent agreement with the theoretical results of Klippenstein and also in reasonable accord with the experimental results of Brucker et al.[23] and Ionov et al.[24]

Another series of important experiments has been carried out by various members of the Reisler group.[33−41] This work examined in detail the product state distributions resulting from the dissociation of NO_2 at various wavelengths. Briefly, they found that the spin−orbit ratios[34,40] for both the NO and O fragments were much lower (colder) than predicted by PST, in accord with measurements of the $O(^3P_j)$ ratios measured by Miyawaki et al.[42] and Knepp et al.[43] and predictions made by Katagiri and Kato.[32] The $^2\Pi_{1/2}$ v=0:v=1 ratios were warmer than those predicted by PST.[33,34] Rotational product state distributions[33−37,41] were found to fluctuate about the PST-predicted values (i) when dissociating at a fixed energy and measuring the distribution of population over the rotational manifold and (ii) when comparing the photofragment yield (PHOFRY) spectra for different rotational levels. On average, the rotational distributions were well-described by phase space theory. In many cases, averaging the product state distributions of the two Λ-doublet components of a given rotational level gave a very good fit to the PST prediction. At low energies, the variations in rotational level populations were attributed to a phenomenon called Ericson fluctuations,[44,45] which arise from interference between overlapping NO_2 absorption resonances. Ericson fluctuations become less important at higher energies (>∼200 cm^{-1}), and there the rotational state fluctuations are attributed to projection of the transition state bending wavefunction onto the product rotational states.[37] Overall, the results of the Reisler group suggest a hierarchy of adiabaticity for describing the order in which the populations in various degrees of freedom become fixed. First vibrations become adiabatic, then rotations, and finally, at long range, the spin−orbit state distributions are fixed.[36,41]

Method. Since the large dissociation laser bandwidth in the Wittig experiments made it difficult to say with precision the energies at which steps in the rate occurred, our initial goal was to develop a method which might determine the energy level structure of the transition state without relying on rate measurement techniques. The new spectroscopic technique involves probing as a function of photolysis energy only the very low kinetic energy products of a dissociation. We have called this new technique zero kinetic energy (ZKE) photofragment spectroscopy. The initial motivation is based on the following reasoning. At first glance, it seems reasonable to assume that energy partitioned into internal modes (i.e., vibrations) in the transition state might remain in internal modes as the reacting system moves on to products. Tlherefore, if the molecule is excited by a photon with just enough energy to access a particular transition state level, all the energy should be partitioned into internal modes, with none left over for translation. In this case, zero kinetic energy (ZKE) products should be formed preferentially when each new energy level in the transition state is accessed. The goal of this experiment was to exploit this notion by measuring the yield of photofragments produced with near-zero kinetic energy as a function of dissociation energy. Peaks in the ZKE spectrum might then be expected to indicate the presence of transition state levels. ZKE photofragment spectroscopy has potential applications to other systems as well. Consider the case of a reaction in which population is partitioned into all energetically accessible quantum states. As a consequence of energy conservation, the rotational and vibrational structure of one fragment can be determined from the ZKE spectrum of the sibling fragment; the ZKE spectrum of the probed fragment would contain a peak corresponding to each energy level of the sibling fragment, which could prove useful in assigning the spectra of unstable

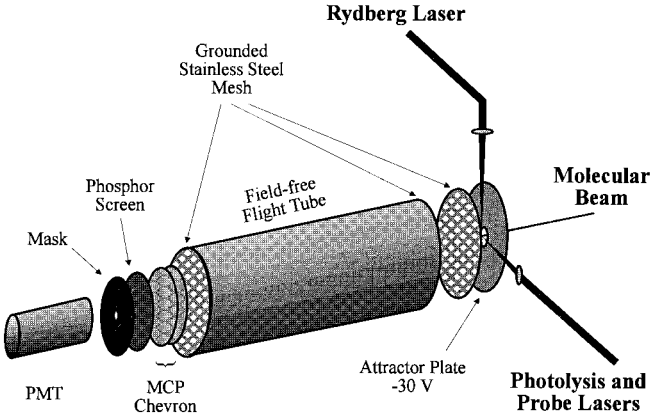

Figure 1. Schematic diagram of the experimental apparatus.

radicals. ZKE photofragment spectroscopy could also be used to determine the dissociation threshold with very high precision, in much the same way that ZEKE photoelectron spectroscopy has offered high resolution in ionization studies.

II. Experimental Section

Our ZKE spectrometer is based on a photofragment imaging apparatus equipped with a microchannel plate(MCP)/phosphor screen detector, as shown in Figure 1. Because the MCP assembly is insensitive to neutral particles, photofragments must be ionized prior to striking the detector. The obvious choice for state-selective ion production is resonance enhanced multiphoton ionization (REMPI). However, in the present experiments the photoproducts of interest have extremely low kinetic energy, and very long flight times ($\sim$360 μs) are required to achieve the necessary resolution of the product scattering spheres. Consequently, ions created via REMPI immediately following dissociation can interact for a long time, resulting in distortion of the ion cloud due to space−charge effects. We eliminate this problem by allowing the photofragments to remain neutral until just before impinging on the detector. This result is accomplished by promoting the photofragment under scrutiny to a long-lived, high-lying Rydberg state a few ns after the dissociation event. These highly excited fragments travel with a center-of-mass velocity equal to that of the molecular beam and pass through a field-free flight tube. The time spent in the flight tube allows the fragment scattering spheres to expand according to their different velocities; the spheres of fragments with low velocities are still very small when they emerge from the flight tube, while those with high velocity are quite large. Due to the strong electric field resulting from the high voltage placed on the detector, the Rydberg-excited photofragments are field ionized upon exiting the field-free region.

The newly formed ions are then accelerated into the position-sensitive MCP. Electrons from the MCP are accelerated into a phosphor screen, and light from the screen is detected by a photomultiplier tube or charge-injection device camera. A mask is placed over the phosphor screen in order to restrict collection of signal to the low kinetic energy photofragments.

For photofragments with very low kinetic energy, the scattering sphere will be small enough that all the signal it produces on the phosphor screen will pass through the mask and be detected. Fragments of higher velocity, however, lie on larger scattering spheres; only a small fraction of the light from these larger spheres (that from photofragments with recoil velocity nearly parallel or antiparallel to the molecular beam) will pass through the mask and reach the PMT.

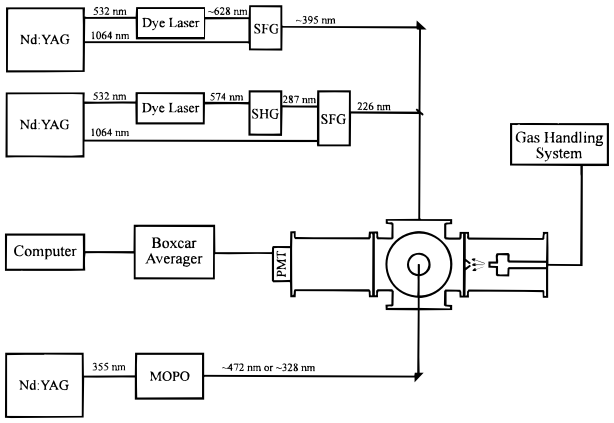

Figure 2. Overview of the laser and electronics components used for ZKE photofragment spectroscopy.

We have successfully probed both the NO($^2\Pi_{1/2}$) and O($^3P_2$) fragments of the NO_2 dissociation using the Rydberg state technique. Although there is some debate as to the factors most important in the production of long-lived Rydberg states, it is generally accepted that lifetimes are extended when population initially excited to a single quantum level is spread over many levels.[46] Application of a static electric field mixes and splits the degenerate l states, moving population from the initially excited level into ones from which fluorescence to a level of low n is unlikely or even forbidden. Mixing of both l and m_l levels can occur as a result of collisions between the excited species and ions. Such collisions are quite likely even in the supersonic molecular beam used in this work, since the collision cross section for Rydberg-excited species is very large, on the order of $\sigma \approx 5 \times 10^{-10}$ cm^2 ($r \approx 0.13$ μm) for $n = 50$.

Rydberg state species are produced using two-color excitation. First, the atom or molecule of interest is excited to an intermediate electronic state using a focused laser, exactly as in a REMPI experiment. A few nanoseconds later, a second laser with different photon energy is used to excite from the resonantly excited state to a high-lying Rydberg state. For the sake of brevity, the two lasers will be termed the "resonant" and "Rydberg" lasers, respectively. Absorption of a photon from the Rydberg laser competes with fragment ionization by absorption of another photon from the resonant laser, so good spatial and temporal overlap of the laser beams is crucial for efficient production of Rydberg-excited species.

Excitation of the Rydberg states is accomplished as follows:

$$\mathrm{O}\,(^3\mathrm{P}_2)\,2\mathrm{p} \xrightarrow{225.65\ \mathrm{nm}} \xrightarrow{225.65\ \mathrm{nm}} \mathrm{O}\,(^3\mathrm{P}_2)\,3\mathrm{p} \xrightarrow{\sim 472\ \mathrm{nm}} \mathrm{O}^{**}$$

$$\mathrm{NO}\,(^2\Pi_{1/2},\, v = 0,\, J'') \xrightarrow{\sim 226\ \mathrm{nm}} \mathrm{NO}\,(^2\Pi_{1/2},\, v = 0,\, J') \xrightarrow{\sim 328\ \mathrm{nm}} \mathrm{NO}^{**} \quad (1)$$

The resonant steps for the probe of both the NO($^2\Pi_{1/2}$) and O($^3P_2$) photofragments require light of approximately 226 nm, which we create as shown in Figure 2 by summing the frequency doubled output of a Quanta-Ray PDL-1 dye laser (rhodamine 590/rhodamine 610 dye mixture, pumped by a 10 Hz Quanta-Ray GCR-270 Nd:YAG laser) with the YAG fundamental. Both nonlinear processes are carried out in a Quanta-Ray WEX-1 using KD*P crystals. The light required for excitation of the photofragment from the resonant state to the high-lying Rydberg state is generated using an optical parametric oscillator (Spectra Physics MOPO-730 pumped by a Spectra Physics GCR-230-10 Nd:YAG laser). We generate the $\sim$472 nm light required

to produce the $O(^3P_2)$ Rydbergs directly with the MOPO. The ~328 nm light for NO Rydberg production requires frequency doubling the MOPO output, using the FDO option of the MOPO.

NO_2 photolysis light (λ = 395−398 nm) is produced by mixing the output of a 10 Hz Quanta-Ray PDL-1 dye laser (DCM dye, pumped by a Spectra-Physics DCR-4 Nd:YAG laser) with the YAG fundamental using a KD*P crystal housed in a Quanta-Ray WEX-1. The laser beams for the dissociation and the resonant step of the probe are copropagated into the chamber and focused into the interaction region using a 75 mm plano-convex lens. We bring the Rydberg laser in from the top of the chamber, perpendicular to the other lasers, and focus it using a 25 cm planoconvex lens. A double Fresnel rhomb placed in the path of the dissociation laser enables rotation of the plane of polarization. We note that the data presented here were taken with the photolysis polarization perpendicular to the direction of propagation of the molecular beam, which in turn was perpendicular to the plane containing the laser beams. Although anisotropy has been observed in the high kinetic energy photofragments from the NO_2 dissociation at relatively low photolysis energy,[2] we observe no significant differences in peak width in the ZKE spectra when we rotate the polarization of the dissociation laser.

We generate the molecular beam by expanding a mixture of 0.5% NO/0.05% O_2 in helium (total pressure = 1000 Torr) into a stainless steel vacuum chamber via a homebuilt, piezoelectrically actuated pulsed nozzle following the design of Proch and Trickl.[47] A 0.5 mm Precision Instruments skimmer is located approximately 1 cm from the 0.3 mm nozzle orifice. Although some of the NO_2 will be in the form of N_2O_4, the dimer is not expected to be a problem for a number of reasons. First, at room temperature and with the low partial pressure used, less than 5% of the NO_2 is in the dimeric form.[48] Second, the absorption cross section of N_2O_4 is more than an order of magnitude less than that of NO_2 in the wavelength region in question.[48,49] Finally, 395−400 nm photons do not have sufficient energy to dissociate N_2O_4 to give O or NO fragments in a single-photon process.[50] Since we detect only the ZKE photofragments, dissociation of N_2O_4 by more than one photon of ~395 nm light or a single photon of 226 nm light is unlikely to contribute to our signal.

A 15 V/cm static electric field is applied to the region in which the lasers crossed the molecular beam. The field was generated between a stainless steel plate at −30 V and a parallel, grounded stainless steel mesh located 2 cm downstream. This field serves a dual function. First, it prevents ions formed by REMPI due to absorption of an additional "resonant" photon from reaching the detector. Second, it facilitates the *l*-mixing required to create long-lived Rydberg states. After Rydberg excitation the excited photofragments, moving with a center-of-mass velocity equal to that of the molecular beam, pass through a 60 cm long field-free flight tube. The Rydberg particles are field ionized after emerging from the flight tube into a region of high electric field (~1200 V/cm) resulting from the negative voltage applied to the front surface of the detector. The ions produced are accelerated into the position-sensitive microchannel plate chevron (Galileo Electro-optics, 4 cm diameter, 12 μm center-to-center distance, 10 μm pore size) coupled to a fast phosphor screen (P-47 phosphor, Galileo Electro-optics). A mask with a 4 mm circular aperture is placed over the phosphor screen to nearly eliminate signal from non-zero kinetic energy fragments from being detected. The light that passes through the hole in the mask is then collected using a RCA 1P21 photomultiplier tube. We use a gated integrator/boxcar averager (SRS Model SR250) to average the signal for 30 shots/wavelength step and then transfer the output of the boxcar to a computer (Gateway 2000, 486/66 MHz) for storage.

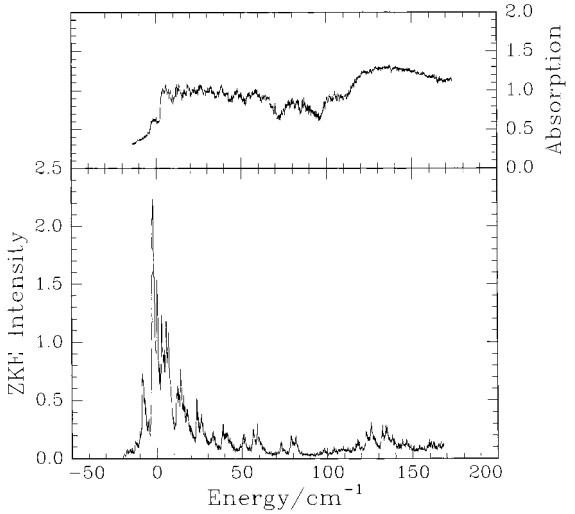

Figure 3. Zero Kinetic Energy spectrum of $O(^3P_2)$ from NO_2 dissociation.

III. Results

Figure 3 shows a typical O atom ZKE photofragment spectrum. The data of Figure 3 have not been corrected for variations in the absorption spectrum of NO_2. Although subsequent figures will make a small correction for the variation in absorption, we point out (1) that every NO_2 molecule that absorbs a photon with energy greater than the dissociation threshold is photodissociated and (2) that under the conditions of our experiment, the NO_2 absorption is essentially saturated. Point 1 follows from the cutoff of fluorescence at the dissociation threshold, observed by Miyawaki, et al.[42] We have confirmed point 2 by monitoring the O^+ signal as a function of NO_2 excitation wavelength; as shown in the upper panel of Figure 3, it is essentially constant above the dissociation threshold and does not show the strong variations observed for much lower powers by Miyawaki et al.[42] Since every molecule which absorbs a photon above the dissociation threshold must necessarily produce an O atom, and since only the $O(^3P_2)$ spin−orbit state is accessible at the photolysis energies studied in this work, the total yield of O atoms is an accurate measure of the number of NO_2 molecules absorbing at a given energy. We also note that the Rydberg laser does not observably deplete the REMPI ion signal. Thus the O^+ signal should give an accurate measurement of the relative absorption. There are slight variations in the absorption (or O^+ signal) given in the upper panel, showing that, for example, the channelplate is not saturated, but the variation is small so that only a small correction needs to be made to the ZKE signal to normalize it for the absorption. For energies above the zero threshold, the correction has been applied to spectra shown in subsequent figures.

Figure 4 shows an expanded O atom ZKE photofragment spectrum in the region near the dissociation threshold. Although most of the NO_2 in the molecular beam is in the ground rotational level, there is some population of excited rotational levels. Since the excited NO_2 molecules have more internal energy than those in the ground rotational level, less energy is required to photodissociate them, and they produce O atoms at

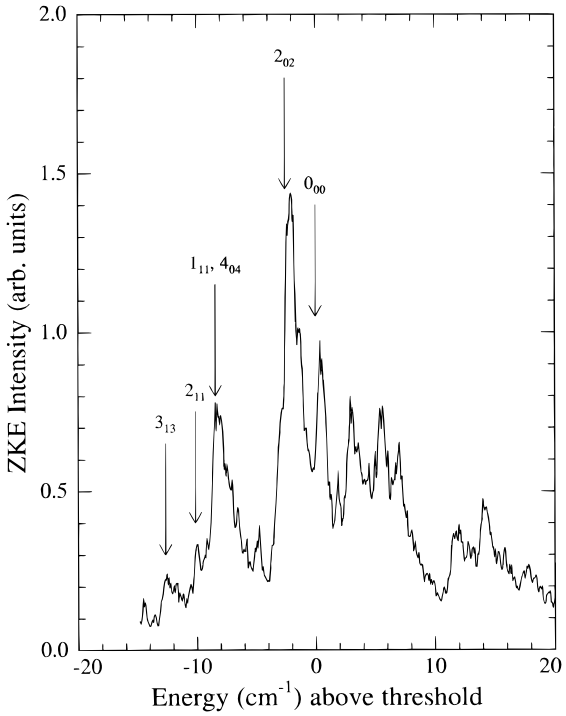

Figure 4. ZKE spectrum near the threshold, showing appearance of different rotational levels of NO_2.

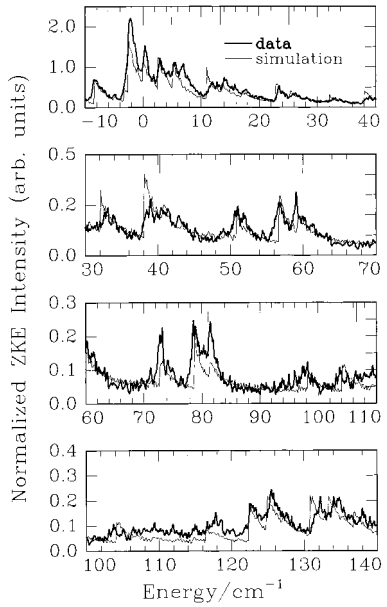

Figure 5. Comparison of phase space theory prediction for a maximum impact parameter of $l_{max} = 5\hbar$ (light line) and the experimental data (heavy line). The long ticks on the top axis of the top three panels give expected positions for the opening of the lower spin−orbit NO rotational channels starting from the ground rotational level of NO_2.

photon energies lower than the dissociation threshold for ground-state NO_2; these are the peaks seen below zero in the ZKE spectrum.

The peaks observed at higher photolysis energies (see Figure 5) correspond to increases in the amount of zero kinetic energy O atoms produced each time a higher rotational level of NO becomes energetically accessible. We note that there are peaks in the spectrum for each rotational level, located at energy $E_J = B_J(J + 1)$ above the dissociation threshold, where B is the rotational constant of free NO. The spin−orbit splitting in NO is approximately 120 cm^{-1}, so the manifold of rotational states associated with the $^2\Pi_{3/2}$ spin−orbit level begins at that point. Note also that the size of the peaks corresponding to the various rotational levels of NO decreases as the photolysis energy increases, presumably because there are more rotational levels over which to distribute the product. This hypothesis will be discussed in more detail in section IV.

IV. Discussion

An important feature of the experimental data in Figure 5 is that a peak appears in the O($^3P_2$) ZKE photofragment spectrum at the exact energy where each NO rotational level becomes energetically allowed. This observation at first suggests that there is not a significant barrier for the production of rotationally excited NO products, since any barrier larger than a few cm^{-1} would preclude production of zero kinetic energy fragments. However, quantitative evaluation of this observation needs to take into account changes in the intensities of the peaks as well as their positions.

It should be noted that there is a relationship between the ZKE spectrum we have recorded and the product state distribution. The ZKE intensity at any energy above threshold is related to the population in that product state that is just energetically accessible at the energy. Product state distributions of NO just above threshold have been recorded by Robra et al.[3] and at higher energies by Robie et al.,[33] Mons and Dimicoli,[56] and Zacharias et al.[57] In general, rotational levels are populated out to the highest level allowed by conservation of energy.

We analyze the ZKE spectrum shown in Figure 3 and expanded in Figure 5 by comparing it to a simulated spectrum; the best fit appears to be for an initial NO_2 beam temperature of 5 K. In addition, the fit assumes that all open product channels within each NO spin−orbit manifold are produced in accordance with phase space theory (PST).[51,52] Because the ratio of NO spin−orbit states is known not to be statistical, we varied the spin orbit ratio to obtain the best fit and found $^2\Pi_{1/2}/^2\Pi_{3/2} = 1.0{:}0.9$. We then calculate the simulated spectrum by a forward convolution program that incorporates the experimental characteristics of our apparatus.

The inputs to the convolution program are the molecular beam divergence (2.5°) and rotational temperature (∼5 K), the radius of the mask (0.2 cm) which determines the energy resolution of 0.5 cm^{-1}, the average beam velocity (1740 m/s), and its dispersion (∼10%). For each dissociation energy bin (0.15 cm^{-1}), for each of 600 iterations, and for each of the initial NO_2 levels and final open NO rotational channels allowed by the beam temperature and total energy, respectively, the program uses a Monte Carlo technique to pick both a beam velocity, determined from the average velocity and dispersion, and a two-dimensional beam center impact position, determined from the divergence. The wavelength and the initial and final rotational level imply a specific recoil velocity, assumed to be isotropic. The "intensity" for each of the iterations is then evenly distributed among 20 points on a sphere whose radius is the product of the recoil velocity and the measured flight time (360 μs). Finally, the fraction of the sphere that strikes the detector within the mask is added to the intensity bin corresponding to the chosen dissociation energy. The dissociation energy is augmented and the procedure repeated until the entire energy range of interest is covered.

Phase space theory assumes a statistical population of product states constrained only by conservation of energy and angular momentum. (The effect of a centrifugal barrier is discussed later.) Energy conservation is thus rather simple: a rotational level can be populated only if its energy does not exceed ϵ, the

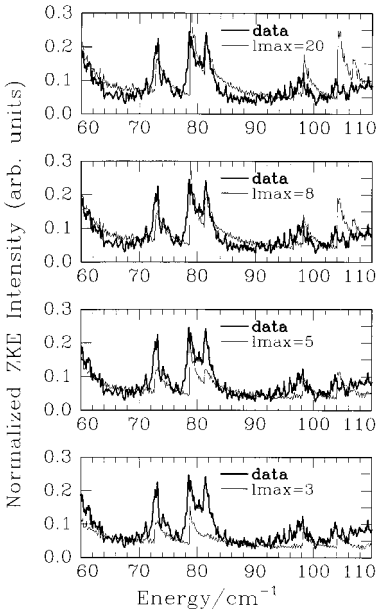

Figure 6. Comparison of data (heavy line) and fit (light line) for various values of l_{max} as indicated.

available energy remaining after the dissociation takes place:

$$\epsilon \geq BJ(J+1) \qquad J \text{ allowed}$$
$$\epsilon < BJ(J+1) \qquad J \text{ forbidden} \tag{2}$$

Angular momentum constraints are somewhat less intuitive. Conservation of angular momentum is given by the vector equation $J_{NO_2} = l + J_{NO} + j_O$, where the magnitudes of the vectors are given as follows. J_{NO_2} is the angular momentum of the excited NO_2 (*after* it has absorbed the photon), l is the orbital angular momentum, and j_{NO} and j_O are the angular momenta of the NO and O products, respectively.

Because we detect $O(^3P_2)$ by the Rydberg technique, $j_O = 2$. For simplicity and to coincide with the notation of ref 52, let $J = J_{NO_2}$ and let $j \equiv j_{NO} + j_O$. Thus, $|J_{NO} - j_O| \leq j \leq J_{NO} + j_O$, and $|J - j| \leq l \leq J + j$. According to this last condition, when $j \geq J$, there are $2J + 1$ possible values of l, whereas when $j < J$, there are $2j + 1$ possible values. Consequently, the degeneracy of each NO product rotational state is a complicated function of the coupling between the various angular momenta, even in the absence of a centrifugal barrier. The presence of a centrifugal barrier further complicates the count by limiting the upper value of l to $l_{max} = \mu v_r b_{max}$, where μ is the reduced mass for the NO and O, v_r is their relative velocity, and b_{max} is the maximum impact parameter consistent with the centrifugal barrier. If, as is often assumed, the centrifugal barrier has a height denoted by $E_{barrier}$, then b_{max} can be determined from the alternate expression

$$E_{barrier} = \frac{l_{max}(l_{max}+1)\hbar^2}{2\mu b_{max}^2} \tag{3}$$

The effect of the centrifugal barrier is to reduce the number of states that contribute to the peak at a particular NO internal level. For high values of l_{max} there will be little diminution of the peak, but when l_{max} is so low that angular momentum can be conserved only for a few combinations of J and j, then the peak will be substantially diminished.

Figure 6 shows an expanded view from 60−110 cm^{-1} of the ZKE spectrum and the predictions made by forward convolution of the phase space theory. We treated the value l_{max} as an adjustable parameter and examined values between 2 and 20 $\hbar$. The figure shows values of 3, 5, 8, and 20 $\hbar$. It is clear both from the figure and from the more extensive calculations that the intensity of the experimentally observed features in this region of dissociation energy (corresponding to $J_{NO} = 6.5$ and 7.5) are substantially diminished from those calculated for values of l_{max} higher than 5$\hbar$. This conclusion is particularly true for levels with the lowest value of $J_{NO_2} = 0.5$. A value of $l_{max} = 5\hbar$ is most consistent with the data.

For the peaks near the dissociation threshold, the ZKE signal reaches a maximum and starts to decrease approximately 0.5 cm^{-1} after the peak onset. (The value of 0.5 cm^{-1} corresponds to the resolution of our instrument.) This energy width implies that the centrifugal barriers for $l > 5$ are greater than 0.5 cm^{-1}. The barriers for $l > 5$ are large enough that, by the time they are surmounted, the scattering spheres are too large to pass unattenuated through the mask on the detector.

It is interesting to see how the value of 0.5 cm^{-1} for the centrifugal barrier at $l = 5\hbar$ corresponds to the barriers that would be calculated by theory. The magnitude of the centrifugal barrier for a particular l is dependent on the form of the attractive potential between the separating fragments and on the amount of energy partitioned into the relative orbital motion of the fragments, which in turn is dependent on l. Formally, the overall potential may be written as

$$V_{total}(R) = V_{attract}(R) + \frac{l(l+1)\hbar^2}{2\mu R^2} \tag{4}$$

In this equation, strictly true for a diatomic system, R is the distance in Jacobi coordinates. The second term on the right-hand side is the energy of the orbital motion of the fragments, also called the centrifugal energy. Since $V_{total}(R) \rightarrow 0$ as $R \rightarrow \infty$, finding the local maximum of $V_{total}(R)$ and evaluating the potential at that point gives the energy of recoil. When $V_{attract}(R)$ has a simple form, for example $V_{attract}(R) = -C_6/R^6$, the local maximum can be found analytically by taking the derivative of $V_{total}(R)$ with respect to R, $dV_{total}(R)/dR$, setting the derivative equal to zero, and then solving for R. This value of R is then substituted back in to eq 4, giving the potential at the maximum. The simple form of the attractive potential $V_{attract}(R) = -C_6/R^6$ allows for a closed form solution for the translational recoil energy $E_{O-NO}(l)$:

$$E_{O-NO}(l) = \left[\frac{l(l+1)\hbar^2}{6\mu(C_6)^{1/3}}\right]^{3/2} \tag{5}$$

Unfortunately, $V_{attract}(R) = -C_6/R^6$ does not accurately describe the O−NO attractive potential,[31,53,54] so this closed form solution should not be used.

Recently, Harding et al.[53] have carried out ab initio calculations of the NO_2 ground state surface for the relatively long range O−NO separations relevant in the dissociation. They find the minimum energy path (MEP) potential on the ab initio surface to be

$$V_{attract}(R) = -\frac{94}{a^4+R^4} - \frac{2680}{b^5+R^5} - \frac{16450}{c^6+R^6} - d(1+gx+kx^2+sx^3+mx^4+nx^5+px^6)\exp(-gx) \tag{6}$$

(eq 3.7 in ref 53). Using this potential, we numerically calculated the centrifugal barriers as a function of l. In eq 6, $V_{attract}(R)$ is given in kcal/mol and R is in au (1 au = 0.529 ×

TABLE 1: Energies and Interfragment Separations of Centrifugal Barriers

l	E_{O-NO} (cm^{-1})	R (au)	l	E_{O-NO} (cm^{-1})	R (au)
0	0	∞	18	6.836	13.126
1	0	∞	19	8.158	12.657
2	0.005	>50	20	9.653	12.235
3	0.021	43.198	21	11.335	11.813
4	0.051	35.504	22	13.216	11.438
5	0.106	30.484	23	15.306	11.109
6	0.191	26.966	24	17.613	10.828
7	0.315	24.339	25	20.138	10.546
8	0.486	22.274	26	22.883	10.359
9	0.714	20.586	27	25.845	10.171
10	1.007	19.225	28	29.022	9.983
11	1.373	18.052	29	32.414	9.843
12	1.824	17.067	30	36.022	9.749
13	2.368	16.223	31	39.844	9.608
14	3.014	15.472	32	43.881	9.514
15	3.773	14.768	33	48.132	9.420
16	4.656	14.159	34	52.601	9.327
17	5.673	13.642	35	57.288	9.233

10^{-10} m), $a = 0.304$ au, $b = 2.035$ au, $c = 3.922$ au, $d = 61.50$ kcal/mol, $g = 2.346$ au^{-1}, $k = -0.397$ au^{-2}, $s = 0.169$ au^{-3}, $m = -0.436$ au^{-4}, $n = 0.276$ au^{-5}, $p = -3.383 \times 10^{-2}$ au, and $x = R - r_0$, where $r_0 = 3.134$ au. The barrier heights and the separations at which they occur are given in Table 1.

The MEP is not quite the same as the angle-averaged potential. During the dissociation process, the molecule is likely to sample the potential at many angles, rather than just the ones along the MEP, so the angle-averaged potential is likely to be more accurate then the MEP. Accordingly, the angle-averaged potential was calculated from the expression for $V(R,\gamma)$ given in ref 53 (R and γ are Jacobi coordinates), using the first-order Legendre polynomial:

$$V(R) = \frac{\langle P_0|V(R,\gamma)|P_0\rangle}{\langle P_0|P_0\rangle} = \frac{\int_0^\pi V(R,\gamma)\sin\gamma\,d\gamma}{\int_0^\pi \sin d\gamma} \quad (7)$$

Since $P_0 = 1$, it need not appear in the explicitly written integral; the factor of $\sin\gamma$ is included as part of the area element for the surface integral. Because the attractive forces between the separating fragments are so small for the values of R at which the centrifugal barriers occur, using the angle averaged potential does not change the calculated barriers significantly. The differences increase with l, but at $l = 30$ the values of E_{O-NO} calculated with the two methods differ by only 0.025 cm^{-1}.

In their study of the NO_2 dissociation near the threshold, Miyawaki et al.[28] did not observe any effects of centrifugal barriers. In a PHOFRY (or PHOFEX) spectrum of a particular j_{NO} level, centrifugal barriers can be expected to have two related effects. First, if the minimum l allowed by angular momentum is greater than zero, the threshold for production of j_{NO} would be higher than expected from the rotational energy of free NO. Second, there would be a separate threshold for each allowed l-level, since the centrifugal barrier is l dependent. Miyawaki et al. measured NO rotational levels up to $j_{NO} = 6.5$ in their experiment. The minimum allowed l for this state is 3, for which the recoil energy is 0.021 cm^{-1}, much too small to resolve with the 0.5 cm^{-1} bandwidth of their laser, so no delay in the onset of the $j_{NO} = 6.5$ PHOFEX signal would be expected, nor was it observed. Although the maximum l allowed in coincidence with $j_{NO} = 6.5$ is 10, and the associated barrier could be resolved by their laser, the unevenness of the PHOFEX spectra makes it very difficult to pick out the onsets for the individual l-levels.

According to the fit and the resolution of our spectra, the recoil energy for $l = 6$ should be greater than 0.5 cm^{-1}. However, according to the Harding potential, E_{O-NO} ($l = 6$) = 0.191 cm^{-1}, and the maximum is expected to occur at 26.97 au (=14.26 Å). At that point, the centrifugal energy for $l = 6$ is 0.333 cm^{-1} and the attraction between the O and NO is 0.142 cm^{-1}. Even if there were no attractive force between the O and NO at 14.26 Å, the centrifugal energy would not be quite sufficient to create a recoil energy of greater than 0.5 cm^{-1}. If the centrifugal barrier is located at somewhat smaller R than predicted by the ab initio potential, the centrifugal energy would be higher (since $E_{cent} \propto 1/R^2$). For this to be the case, however, the attractive potential must have a slightly different shape, being slightly less attractive at large R. Since the goal of Harding et al. was to model the potential at $R < \sim 11$ au, slight inaccuracies in the fit to the ab initio potential at large R are not unexpected.

Another complication in the calculation of the long-range potential is the participation of other electronic surfaces that may have attractive, shallow wells at long range. Such wells have been proposed to account for the increase in the density of states just below the threshold for NO_2 dissociation.[17-22] The rough agreement between the magnitude of the $l = 6$ barrier calculated from the Harding potential and the barrier we observe suggests that the wells, if present, are not deeper than a few tenths of a wavenumber for the internuclear separation corresponding to this value of l.

The Signature of the Transition State

Increases in the amount of ZKE signal at the energies where step-like changes in the rate were observed by Brucker et al.[23] and Ionov et al.[24] and were taken to indicate that the transition state tightens as the energy increases. This notion is in agreement with the calculations of Katagiri and Kato.[32] In the Katagiri and Kato transition state, an *adiabatic* dissociation would imply that molecules with just enough energy to access a particular transition state level would produce fragments with a considerable amount of translational energy so that we should not have observed any ZKE photoproducts. However, our observation that there is a peak in the ZKE spectrum at the exact energy where each NO state just becomes accessible implies that either the transition state must be still quite loose or that there must be significant nonadiabatic transitions between channels leading to different NO product states.

V. Conclusions

The ZKE photofragment method presented above provides a technique that is suitable for finding dissociation thresholds, examining the nonadiabatic coupling between transition states and final states, and for determining the maximum orbital angular momentum of a dissociation and thereby providing information about the attractive part of the potential at long range. The potential developed by Harding et al.,[53] despite not having been developed to address the long range at which our experiments are most sensitive, appears to provide a reasonable description.

The oxygen atom ZKE photofragment spectrum was well-fit by a product state distribution predicted by PST. This result implies that extensive nonadiabatic interactions take place in the region of the transition state. It was found that a maximum l value of $5\hbar$ had to be imposed in order for the phase space theory simulation to match the measured spectrum, implying

that the centrifugal barriers associated with $l > 5$ give rise to a recoil energy greater than the $\sim$0.5 cm^{-1} resolution of the peaks observed in our spectrum.

Acknowledgment. This work was supported by the Department of Energy under Grant DE-FG02-88ER13934. The authors thank Simon North both for discussions about phase space theory and for experimental assistance, Larry Harding for making available to us a preprint of ref 53, and Darcy Peterka for construction of the molecular beam valve and electronics.

References and Notes

(1) Jost, R.; Nygård, J.; Pasinski, A.; Delon, A. *J. Chem. Phys.* **1996**, *105*, 1287.
(2) Butenhoff, T. J.; Rohlfing, E. A. *J. Chem. Phys.* **1993**, *98*, 5469.
(3) Robra, U.; Zacharias, H.; Welge, K. H. *Z. Phys. D* **1990**, *16*, 175.
(4) Changlong, N.; Hua, L.; Pfab, J. *J. Phys. Chem.* **1993**, *97*, 7458.
(5) Suzuki, T.; Hradil, V. P.; Hewitt, S. A.; Houston, P. L.; Whitaker, B. J. *Chem. Phys. Lett.* **1991**, *187*, 257.
(6) Hradil, V. P.; Suzuki, T.; Hewitt, S. A.; Houston, P. L.; Whitaker, B. J. *J. Chem. Phys.* **1993**, *99*, 4455.
(7) Harrison, J. A.; Yang, X.; Rösslein, M.; Felder, P.; Huber, J. R. *J. Phys. Chem.* **1994**, *98*, 12260.
(8) Busch, G. E.; Wilson, K. R. *J. Chem. Phys.* **1972**, *56*, 3638.
(9) Kawasaki, M.; Sato, H.; Fukuroda, A.; Kikuchi, T.; Kobayashi, S.; Arikawa, T. *J. Chem. Phys.* **1987**, *86*, 4431.
(10) Mons, M.; Dimicoli, I. *Chem. Phys. Lett.* **1986,** *131*, 298.
(11) Mons, M.; Dimicoli, I. *J. Chem. Phys.* **1989,** *90*, 4037.
(12) Gillispie, G. D.; Khan, A. U.; Wahl, A. C.; Hosteny, R. P.; Krauss, M. *J. Chem. Phys.* **1975**, *63*, 3425.
(13) Jackels, C. F.; Davidson, E. R. *J. Chem. Phys.* **1976**, *64*, 2908.
(14) Jackels, C. F.; Davidson, E. R. *J. Chem. Phys.* **1976**, *65*, 2941.
(15) Leonardi, E.; Petrongolo, C.; Hirsch, G.; Buenker, R. J. *J. Chem. Phys.* **1996**, *105*, 9051 and references therein.
(16) Leonardi, E.; Petrongolo, C. *J. Chem. Phys.* **1997**, *106*, 10066 and references therein.
(17) Delon, A.; Jost, R.; Lombardi, M. *J. Chem. Phys.* **1991**, *95*, 5701.
(18) Delon, A.; Dupre, P.; Jost, R. *J. Chem. Phys.* **1993**, *99*, 9482.
(19) Delon, A.; Georges, R.; Kirmse, B.; Jost, R. *Faraday Discuss.* **1995**, *102*, 117.
(20) Delon, A.; Georges, R.; Jost, R. *J. Chem. Phys.* **1995,** *103*, 7740.
(21) Miyawaki, J.; Yamanouchi, K.; Tsuchiya, S. *J. Chem. Phys.* **1994**, *101*, 4505.
(22) Ionov, P. I.; Bezel, I.; Ionov, S. I.; Wittig, C. *Chem. Phys. Lett.* **1997**, *272*, 257.
(23) Brucker, G. A.; Ionov, S. I.; Chen, Y.; Wittig, C. *Chem. Phys. Lett.* **1992**, *194*, 301.
(24) Ionov, S. I.; Brucker, G. A.; Jacques, C.; Chen, Y.; Wittig, C. *J. Chem. Phys.* **1993**, *99*, 3420.
(25) Baer T.; Hase, W. L. *Unimolecular Reaction Dynamics: Theory and Experiments*, Oxford: New York, 1996.
(26) Delon A.; Jost, R. *J. Chem. Phys.* **1991**, *95*, 5686.
(27) Johns, J. W. C.; Reid, J.; Lepard, D. W. *J. Mol. Spectrosc.* **1977**, *65*, 155.
(28) Miyawaki, J.; Yamanouchi, K.; Tsuchiya, S. *J. Chem. Phys.* **1993**, *99*, 254.
(29) Miyawaki, J.; Yamanouchi, K.; Tsuchiya, *S. J. Chem. Phys.* **1994**, *100*, 4716.
(30) Wittig, C.; Ionov, S. I. *J. Chem. Phys.* **1994**, *100*, 4714.
(31) Klippenstein, S. J.; Radivoyevitch, T. *J. Chem. Phys.* **1993**, *99*, 3644.
(32) Katagiri, H.; Kato, S. *J. Chem. Phys.* **1993**, *99*, 8805.
(33) Robie, D. C.; Hunter, M.; Bates, J. L.; Reisler, H. *Chem. Phys. Lett.* **1992**, *193*, 413.
(34) Hunter, M.; Reid, S. A.; Robie, D. C.; Reisler, H. *J. Chem. Phys.* **1993**, *99*, 1093.
(35) Reid, S. A.; Brandon, J. T.; Hunter, M.; Reisler, H. *J. Chem. Phys.* **1993**, *99*, 4860.
(36) Reid, S. A.; Robie, D. C.; Reisler, H. *J. Chem. Phys.* **1994**, *100*, 4256.
(37) Reid, S. A.; Reisler, H. *J. Chem. Phys.* **1994**, *101*, 5683.
(38) Reid, S. A.; Sanov, A.; Reisler, H. *Faraday Discuss.* **1995**, *102*, 129.
(39) Sanov, A.; Bieler, C. R.; Reisler, H. *J. Phys. Chem.* **1995**, *99*, 7339.
(40) Sanov, A.; Bieler, C. R.; Reisler, H. *J. Phys. Chem.* **1995**, *99*, 13637.
(41) Reid S. A.; Reisler, H. *J. Phys. Chem.* **1996**, *100*, 474.
(42) Miyawaki, J.; Tsuchizawa, T.; Yamanouchi, K.; Tsuchiya, S. *Chem. Phys. Lett.* **1990,** *165*, 168.
(43) Knepp, P. T.; Terentis, A. C.; Kable, S. H. *J. Chem. Phys.* **1995**, *103*, 194.
(44) Ericson, T. *Phys. Rev. Lett.* **1960,** *5*, 430.
(45) Hodgson, P. E. *Nuclear Reactions and Nuclear Structure;* Clarendon Press: Oxford, 1971.
(46) Chupka, W. A. *J. Chem. Phys.* **1993**, *98*, 4520.
(47) Proch, D.; Trickl, T. *Rev. Sci. Instrum.* **1989,** *60*, 713.
(48) Bass, A. M.; Ledford, Jr., A. E.; Laufer, A. H. *J. Res. Natl. Bur. Stand.* **1976,** *80A*, 143.
(49) Hall T. C.; Blacet Jr., F. E. *J. Chem. Phys.* **1952**, *20*, 1745.
(50) Stull, D. R.; Prophet, H. *JANAF Thermochemical Tables;* NSRDS-NBS 37; U.S. Government Printing Office, Washington, DC, 1971.
(51) Pechukas, P.; Light, J.; Rankin, C. *J. Chem. Phys.* **1966**, *44*, 794.
(52) North S. W.; Hall, G. E. *J. Chem. Phys.* **1996,** *104*, 1864.
(53) Harding, L. B.; Stark, H.; Troe, J.; Ushakov, V. G. *J. Chem. Phys.* **1998**. In press.
(54) Troe, J. *Faraday Discuss.* **1995**, *102*, 229.
(55) Rabache, P. *J. Quant. Spectrosc. Radiat. Transfer* **1977**, *17*, 673.
(56) Mons, M.; Dimicoli, I. *Chem. Phys. Lett.* **1989**, *130*, 307.
(57) Zacharias; H., Geilhaupt, M.; Meier, K.; Welge, K. H. *J. Chem. Phys.* **1981**, *74*, 218.